IEEE Access
Multidisciplinary ⋮ Rapid Review ⋮ Open Access Journal

Received August 9, 2019, accepted August 18, 2019, date of publication August 23, 2019, date of current version September 9, 2019.

Digital Object Identifier 10.1109/ACCESS.2019.2937180

Stability Enhancement and Direct Speed Control of DFIG Inertia Emulation Control Strategy

HAOSHU SHAO[1], (Student Member, IEEE), XU CAI[1], ZHENG LI[2], DANGSHENG ZHOU[3], SUJUAN SUN[4], LIANG GUO[4], YUNFENG CAO[1], AND FANGQUAN RAO[1]

[1]Wind Power Research Center, School of Electronic Information and Electrical Engineering, Shanghai Jiao Tong University, Shanghai 200240, China
[2]College of Information Science and Technology, Donghua University, Shanghai 201620, China
[3]Shenzhen Hopewind Electric Co., Ltd, Shenzhen 518000, China
[4]State Grid Electric Power Research Institute (NARI Group Corporation), Nanjing 211000, China

Corresponding author: Xu Cai (xucai@sjtu.edu.cn)

This work was supported by the National Key Research and Development Program of China under Grant 2018YFB0904005.

ABSTRACT With the increasing penetration of renewable energy generators in power grid, traditional vector control (VC) strategy for double fed induction generator (DFIG) is unable to provide extra active power support to grid because DIFG inertia is made decoupled from grid frequency fluctuations. To solve this problem, Virtual Synchronous Generator (VSG) control strategy as well as Inertial Synchronization Control (ISynC) strategy are proposed for DFIG rotor side converter (RSC) and grid side converter (GSC) respectively, so that DFIG rotor speed will experience an acceleration or a deceleration process to release or absorb the kinetic energy stored in DFIG wind turbines, which can prevent grid frequency from deep drop or increase. However, VSG-ISynC control strategy has its limitations in that rotor speed may lose its stability when large load is added into power system, at the same time, the secondary frequency drop is serious if rotor speed has decreased lower than the admissible minimum value. To address this issue, a modified VSG (M-VSG) control strategy is proposed by dynamically changing the *P-f* droop coefficient of conventional VSG control strategy, aiming to expand the stability boundary of DFIG operation. Additionally, an extra rotor speed closed loop is added into VSG control strategy, which can significantly reduce serious frequency secondary drop by controlling rotor speed directly. Simulation and hardware-in-loop (HIL) verification are both carried out in RTDS & GH Bladed co-simulation research platform to verify the effectiveness of proposed M-VSG control strategy.

INDEX TERMS Double fed induction generator (DFIG), inertial synchronization control strategy, modified control strategy, stability boundary, secondary frequency drop, virtual synchronous generator control strategy.

I. INTRODUCTION

With the rapid development of sustainable clean energy, the penetration of wind generators in power grid has increased significantly, which has put forward higher requirements for wind turbine generators to participate in power system frequency regulation [1]–[4]. At the same time, the percentage of double fed induction generator (DFIG) wind turbines in modern wind power system has also increased rapidly for their unique structure and high efficiency. However, most DFIG wind turbine generators (WTG) are connected to grid via electronic converters, inertia is made decoupled from grid frequency [5], [6], thus it is necessary to add inertia emulation control in DFIG WTG to improve the integration performance of wind turbines.

In order to meet the requirement of DFIG WTG frequency regulation, many scholars have conducted comprehensive researches, aiming to control DFIG WTG like traditional synchronous generators (SG), because SGs are capable of releasing the generator kinetic energy to grid or absorbing extra energy from grid during grid disturbances [1], [7]–[15]. One of the inertia emulation control strategies is to add grid frequency differential signals (i.e., df/dt) and the signal of frequency deviation beyond nominal value (i.e., Δf) into the power reference of DFIG WTG rotor side converter (RSC) [7]–[9], so that the fluctuation of grid frequency is able to influence the output of DFIG active power, forcing DFIG WTG to produce extra power to support grid frequency at

The associate editor coordinating the review of this article and approving it for publication was Shiwei Xia.

the cost of decreasing its rotor speed. However, this inertia emulation control strategy still has its obvious limitations in that DFIG WTG still need phase locked loop (PLL) to synchronize with grid, as power grid becomes weak, its robustness and tracking accuracy cannot be guaranteed and the entire control system is likely to be unstable [10], [11].

To conquer the problem of weak grid stability, virtual synchronous generator (VSG) control strategy is proposed in [1], [12]–[16], where swing equation of traditional SG is utilized instead of PLL to synchronize with power grid, RSC is externally embodied as a voltage source, DFIG WTG is able to actively response to frequency fluctuations. At the same time, the built-in droop and inertia characteristics of VSG control strategy can provide better performance in weak grid condition [1], [12], [13]. There are usually two independent control loops in VSG control strategy, active power control loop is responsible for mimicking the rotor motion equation to regulate active power, while reactive power control loop is used to regulate DFIG reactive power by controlling the amplitude of stator voltage [14], [15].

Considering that the stator of DFIG WTG is connected directly to grid, DFIG rotor is linked to grid via a back-to-back converter, power can be delivered from DFIG to grid through both RSC and grid side converter (GSC). VSG control is only effective in RSC but cannot be applied to GSC, weak grid operating stability will still be deteriorated if GSC continues to adopt traditional vector control (VC) strategy. Based on that, a novel inertial synchronization control (ISynC) is proposed in [16], where the dynamic equation of dc link voltage is compared with the rotor motion equation and analogy control is then carried out according to the principle of power system similarity, so that the fluctuations of grid frequency can be well reflected on DFIG dc link voltage. Considering that ISynC does not need PLL for coordinate transformation, GSC is embodied as a voltage source, so the combination of VSG for RSC and ISynC for GSC can achieve the best control results in both frequency damping and weak grid operating stability [17].

There have been many works involving the modeling and analysis of VSG and ISynC control strategy [13], [16]–[19]. The detailed small signal model of ISynC control strategy is built in [16], a PLL-less control strategy is then applied to Type-IV wind turbine with the help of GSC ISynC control strategy. Four main types of inertia emulation control strategies are compared in [17] in terms of inertia response performance, weak grid operation stability, secondary frequency drop, and wind tower fatigue load. However, such models and comparisons are mainly focused on the current inertia emulation control strategies and cannot settle the problem of instability in load transient.

Small signal sequence impedance model is built in [18] to analyze the sequence impedance characteristics between VSG and traditional VC control strategies. Besides, small signal models of VSG and droop control strategies are built in [13] and [19] to compare their differences in frequency transient responses during a small loading transition. However, simulation results can only validate that VSG has a better stability characteristic in weak grid condition, the stability issue during large load changes is less studied. The damping characteristics of VSG and ISynC control strategy is not infinite, when load disturbances are large enough, it is likely to lose its stability and get out of control. So it is of urgent need to propose a new modified VSG control strategy to expand DFIG stability boundary under large load changes.

Additionally, another serious problem faced by all inertia emulation control strategies is frequency secondary drop [20], [21]. The definition is that when DFIG rotor speed has decreased below the permitted minimum value, the rotor speed protection block will disable the function of droop control, which will lead to the increase of rotor speed, although rotor speed can be protected from continuing drop, the sudden change of control topology will cause serious frequency secondary drop, which will impose adverse impacts on frequency stability.

A possible modification of VSG control strategy to avoid frequency secondary drop is proposed in [21], four compensational methods are introduced to avoid the instantaneous decrease of the active power to prevent frequency secondary drop. Similarly, reference [22] proposes a control strategy to reduce frequency secondary drop by virtual inertia planning. However, this control strategy can only reduce the level of frequency secondary drop, it cannot eventually avoid grid frequency from secondary drop because the rotor speed is totally out of control during the whole process of inertia response, the best way to avoid frequency secondary drop is to control rotor speed directly instead of just reducing frequency drop level.

In this paper, we mainly focus on the possible modification of conventional VSG-ISynC control strategy. Basic stability analysis is firstly conducted based on VSG-ISynC control strategy, revealing the mathematical mechanism behind stability analysis and then pointing out the stability criterion for VSG-ISynC control strategy. In order to overcome the problem of limited stability boundary and frequency secondary drop, a modified VSG-ISynC control strategy (M-VSG) is proposed in this paper, which can improve the stability boundary by dynamically changing the value of droop coefficient. Moreover, a specific rotor speed control loop is added into the VSG synchronization control loop, so that the frequency secondary drop can be prevented by directly controlling DFIG rotor speed. A systematic control strategy from low wind speed to high wind speed is finally proposed based on the two modifications of VSG-ISynC control strategy. Afterwards, the quantitative analysis and state space equation is built for M-VSG control strategy, impacts of droop coefficient on system stability is investigated by the eigenvalue loci analysis. Finally, the effectiveness of proposed M-VSG control strategy in terms of expanding system stability boundary and avoiding frequency secondary drop is verified on RTDS and GH Bladed co-simulation research platform.

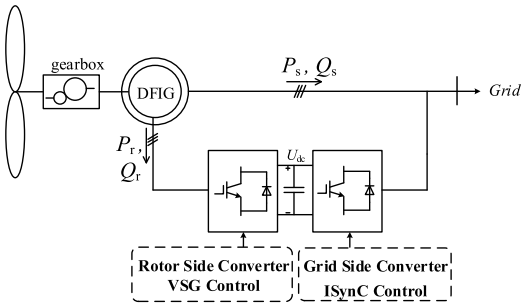

FIGURE 1. Diagram of VSG control for RSC and ISynC control for GSC.

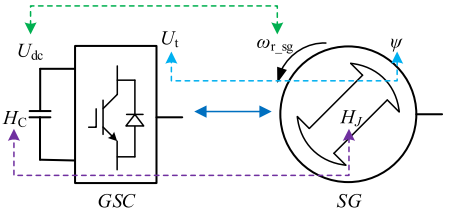

FIGURE 2. Analogy relations between GSC and SG.

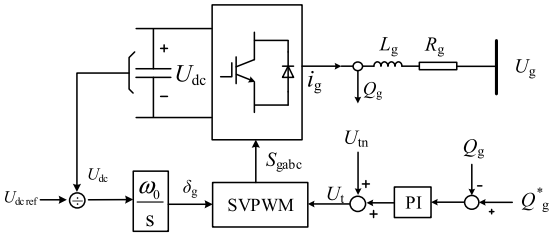

FIGURE 3. Control diagram of ISynC control strategy for DFIG GSC.

The rest of this paper is organized as followed: Section II explains the detailed control strategy of VSG-ISynC control strategy. Section III includes a detailed stability analysis of VSG-ISynC control strategy on its damping characteristics and system stability boundary, revealing the mathematical mechanism of stability and then pointing out the major limitations of conventional VSG-ISynC control strategy. A modified VSG control strategy (M-VSG) is proposed in Section IV. Section V includes the quantitative analysis and state space modeling of M-VSG control strategy. Section VI builds a co-simulation research platform based on real-time digital simulator (RTDS) and GH Bladed simulation software, simulation and RTDS hardware-in-loop (HIL) verifications are carried out in Section VII. Section VIII briefly draws several conclusions.

II. BASIC THEORY OF VSG-ISynC CONTROL STRATEGY

Among all the inertia emulation control strategies, the combined control strategy of VSG-ISynC is widely accepted [16], detailed control diagram of VSG-ISynC strategy is shown in Fig.1, where DFIG RSC adopts VSG strategy and GSC is controlled under ISynC strategy. P_s and Q_s are the stator active power and reactive power, P_r and Q_r are the rotor active power and reactive power. The advantage of VSG-ISynC coordinated control strategy is that neither of them need PLL to synchronize with gird, VSG-ISynC has a better weak grid stability performance than other traditional strategies.

The core of ISynC is to compare the dynamic equation of dc link capacitance with the rotor motion equation, so that the variation tendency of dc link voltage is strictly synchronized with that of grid frequency, analogy control is carried out according to the principle of power system similarity, considering that power loss in GSC can be neglected, then dc link voltage U_{dc} and GSC active power P_g can be expressed as:

$$2H_C(U_{dc}\frac{dU_{dc}}{dt}) = P_r - P_g \tag{1}$$

$$P_g = \frac{U_t U_{dc} U_g}{x_g}\sin\delta \tag{2}$$

where P_r and P_g are active power of RSC and GSC, H_C is the capacitance inertia time constant, U_t is GSC modulation voltage, U_{dc} is dc link voltage, U_g is grid voltage, x_g is the equivalent reactance between GSC and grid, δ stands for the angle that GSC voltage leads grid voltage.

On the other hand, SG rotor swing equation and active power are described as:

$$2H_J\left(\omega_{r\_sg}\frac{d\omega_{r\_sg}}{dt}\right) = P_M - P_{em} \tag{3}$$

$$P_{em} = \frac{\psi\omega_r U_g}{x_{sg}}\sin\delta_{sg} \tag{4}$$

where P_M and P_{em} are SG input mechanical power and active power, ω_{r_sg} is SG rotor speed, H_J is SG rotor inertia time constant, ψ is SG rotor flux linkage, x_{sg} and δ_{sg} are SG equivalent reactance and power angle.

When we put (1) to (4) together we can find that the expression of dc link voltage in (1) is similar to the equation of rotor speed in (3). Furthermore, GSC modulation voltage U_t in (2) can be analogous to rotor flux linkage ψ in (4) while capacitance inertia time constant H_C in (1) can be analogous to SG rotor inertia time constant H_J in (3). The relationship among the above variables and control diagram of ISynC are shown in Fig.2-3. Phase angle of GSC output voltage δ_g is obtained through integrator, while dynamic adjustment of the GSC reactive power is realized by controlling GSC modulation voltage U_t, U_{tn} is the rated GSC modulation voltage, L_g and R_g are the grid inductance and resistance.

Detailed control strategy of RSC VSG control strategy is shown in Fig.4, where the main control concept is to mimic the behavior of traditional synchronous generator, which can provide extra power support when grid frequency experiences fluctuations. The definition of DFIG equivalent electromotive force $\boldsymbol{E}_r^{eq}$ and equivalent power angle δ_{eq} are given in [17], which means that the expression of DFIG stator voltage is similar to the stator voltage of traditional SG, DFIG active power can be regulated through the control of equivalent power angle δ_{eq}, while the adjustment of the amplitude of $\boldsymbol{E}_r^{eq}$ is equal to the control of DFIG reactive power.

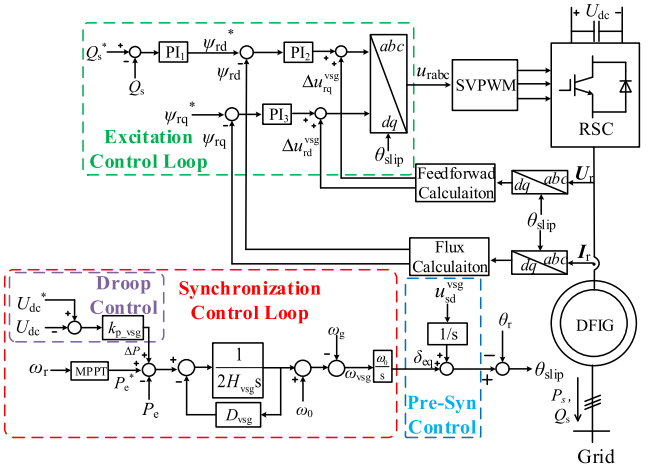

FIGURE 4. Control diagram of VSG for DFIG RSC.

In VSG synchronization control loop, ω_r is DFIG rotor speed, ΔP is the output of droop control, P_e^* is calculated in MPPT module and k_{p_vsg} is defined as *P-f* droop coefficient. Since GSC is controlled under ISynC strategy, so we can easily get the signal of grid frequency fluctuations through dc link voltage. The unbalanced power between active power reference and DFIG active power P_e causes the transient of VSG rotor speed ω_{vsg}. H_{vsg} and D_{vsg} are virtual rotor inertia time constant and virtual damping factor for RSC VSG control strategy, the slip angle θ_{slip} is the difference between VSG equivalent power angle δ_{eq} and DFIG rotor angle θ_r. VSG rotor rotating reference frame is ultimately determined by ω_{vsg} and δ_{eq}.

In VSG excitation control loop, DFIG rotor flux linkage ψ_r is oriented at VSG rotor rotating reference frame, the component of ψ_r in q-axis ψ_{rq} is kept to zero while d-axis component ψ_{rd} is regulated to meet the requirement of DFIG reactive power. Pre-Syn Control is only enabled for DFIG wind turbine to synchronize with grid before integration.

III. STABILITY ANALYSIS OF VSG-ISynC CONTROL STRATEGY

A. DAMPING CHARACTERISTISCS OF VSG-ISynC CONTROL STRATEGY

Based on the theory proposed in the previous chapter, DFIG equivalent electromotive force $\boldsymbol{E}_r^{eq}$ and equivalent power angle δ_{eq} have similar characteristics as traditional synchronous generator. In VSG synchronization control loop, the differential equation of δ_{eq} is given as:

$$s\delta_{eq} = \frac{P_{ref} - P_e}{2H_{vsg}s + D_{vsg}} + \omega_0 - \omega_g \tag{5}$$

where ω_g is the angular frequency of the grid, ω_0 is the rated grid angular frequency, P_{ref} is calculated according to the MPPT curve and droop control, because dc link voltage is strictly synchronized with grid frequency, so we can easily get the function of P_{ref} and P_e as

$$\begin{cases} P_{ref} = k_{opt}\omega_r^3 + k_{p\_vsg}k_{dc}(\omega_0 - \omega_g) \\ P_e = \dfrac{E_r^{eq}U_s}{X_{eq}}\sin\delta_{eq} = P_0\sin\delta_{eq} \end{cases} \tag{6}$$

where k_{opt} is defined as power coefficient, k_{dc} is the proportional coefficient between grid frequency and dc link voltage, U_s is DFIG stator voltage and X_{eq} refers to the equivalent reactance between DFIG and power grid. It is worth mentioning that a special droop control loop is added in the calculation of power reference P_{ref} to emulate the *P-f* droop control. Meanwhile, when DFIG is operating at steady state, the Pre-Syn control is not included in δ_{eq} differential equation and δ_{eq} remains at a constant value, so we get the function of DFIG active power $P_0\sin\delta_{eq}$ in steady state as

$$P_0\sin\delta_{eq} = k_{opt}\omega_r^3 + k_{p\_vsg}k_{dc}(\omega_0 - \omega_g) + (\omega_0 - \omega_g)(2H_{vsg}s + D_{vsg}) \tag{7}$$

DFIG rotor swing equation function is given as

$$2H_{DFIG}\frac{d\omega_r}{dt} = \frac{P_M}{\omega_r} - \frac{P_0\sin\delta_{eq}}{\omega_r} - D_{DFIG}\omega_r \tag{8}$$

where P_M is the mechanical power from DFIG wind turbine, H_{DFIG} and D_{DFIG} are DFIG rotor inertia time constant and its damping factor, ω_r experiences no variation in steady state, that means $d\omega_r/dt = 0$, so we get another equation to express DFIG output power

$$P_0\sin\delta_{eq} = P_M - D_{DFIG}\omega_r^2 \tag{9}$$

Meanwhile, the expression of P_M in (8) and (9) satisfies the following equation of output mechanical power

$$P_M = \frac{1}{2}\rho\frac{C_p}{\lambda^3}\pi R^5\omega_r^3 \tag{10}$$

where ρ is air density, C_p is wind turbine power coefficient, R is the blade radius, λ is tip-speed ratio. When DFIG WTG is controlled under MPPT power curve, the relationship between the optimal tip-speed ratio λ_{opt} and optimal turbine angular velocity ω_M^{opt} is

$$\lambda_{opt} = \frac{\omega_M^{opt}R}{v_w} \tag{11}$$

In (11), v_w is the wind speed of DFIG WTG, so we can get the function of P_M by substituting optimal tip-speed ratio λ_{opt} and optimal wind turbine power coefficient C_p^{opt} into (10), as is shown in (12)

$$P_M = \frac{1}{2}\rho\frac{C_p^{opt}}{\lambda_3^{opt}}\pi R^5\omega_r^3 = k_M\omega_r^3 \tag{12}$$

Substituting (12) into (9) yields another equivalent function of DFIG output power as

$$P_0\sin\delta_{eq} = k_M\omega_r^3 - D_{DFIG}\omega_r^2 \tag{13}$$

Note that (7) and (13) are equivalent expression of DFIG output power, so the relationships between DFIG rotor speed

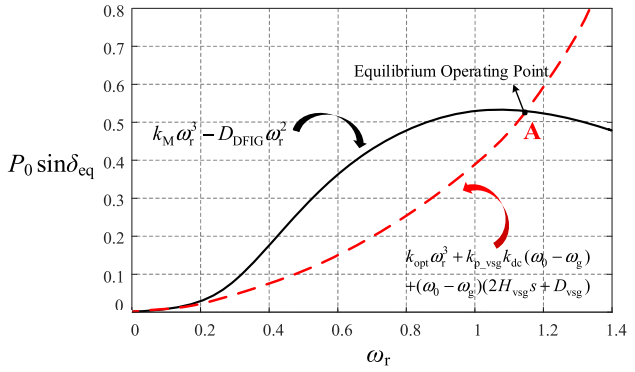

FIGURE 5. Schematic diagram of equilibrium operating point.

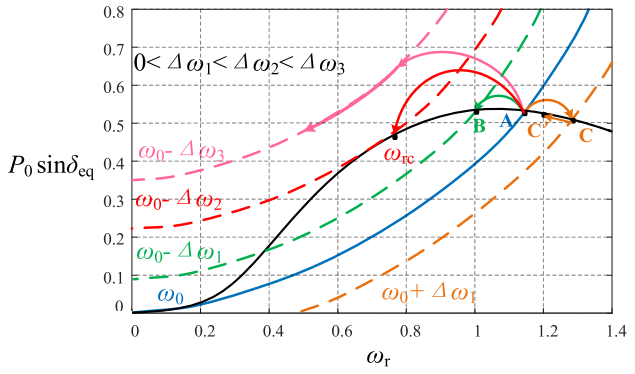

FIGURE 6. Schematic diagram of equilibrium operating point under frequency deviations.

ω_r and grid frequency ω_g can be drawn easily when we put (7) and (13) in one single plot, where rotor speed ω_r is selected as x-axis and y-axis represents DFIG active power, as is shown in Fig.5. The black solid line stands for the expression of active power in (13) while the red dashed line stands for the expression of active power in (7), the intersection point between the black solid line and the red dashed line is the equilibrium operating point for DFIG WTG.

For VSG-ISynC control strategy, the most important advantage is its damping characteristics, which is similar to traditional synchronous generator. When extra load is added into DFIG power system, then grid frequency is expected to decrease, if DFIG WTG is controlled under traditional vector control for both RSC and GSC, no extra power can be extracted to support power grid. However, if DFIG is controlled under VSG-ISynC strategy, the process of inertia response can be reflected in Fig.6. (i.e. dashed line of $\omega_0 - \Delta\omega_1$). The equilibrium operating point will experience an up-down transient process and move form original point A to point B, which indicates that DFIG generator will lower its speed value to release kinetic energy to power grid. However, if grid frequency has decreased over a permitted range, then the kinetic energy stored in DFIG WTG will not be enough to provide frequency support. As is shown in Fig.6, when frequency drop is $\Delta\omega_3$, then there will be no intersection point between the solid line and the dashed line, in which case rotor speed will continually decrease until totally out of control. It can be deduced that for a given wind speed, there exists a critical operating point ω_{rc}, ω_{rc} is the operating point where the solid line is tangent to the dashed line. If rotor speed has decreased lower than ω_{rc}, then VSG-ISynC control strategy will lose its stability.

Similarly, if grid frequency rises, the equilibrium point will move to the opposite direction compared with frequency drop until reaching a new equilibrium point, where rotor speed ω_r is obviously increased to absorb active power, once rotor speed has increased over 1.2pu, DFIG WTG pitch angle controller will be activated to keep rotor speed constant at 1.2pu. As is shown in Fig.6, once grid frequency rises, operating point will move from A to C, but rotor speed has exceeded 1.2pu in point C, so pitch angle will increase accordingly to lower rotor speed around 1.2pu, DFIG WTG will finally operate at C' instead of C. Different from frequency drop situation, no matter how serious the frequency rise is, DFIG can always find its new equilibrium operating point in frequency rise situation.

B. MATHEMATICAL MECHANISM ANALYSIS OF VSG-ISynC STABILITY

The principle of VSG-ISynC stability analysis is introduced in the previous section based on a $P_0 \sin\delta_{eq} - \omega_r$ plot, this analysis method is visualized and very easy to understand, operation stability can be well judged by the number of intersection points in $P_0 \sin\delta_{eq} - \omega_r$ plot, mathematical analysis is necessary in order to perfect this stability analysis theory.

The output active power of DFIG WTG can be described in two independent equations, equation (7) is derived from DFIG VSG control strategy, while equation (13) is derived from DFIG rotor swing equation function, when we put the two equations together, the intersection point is equilibrium operating point, which is exactly the solution of the following equation

$$k_M\omega_r^3 - D_{DFIG}\omega_r^2 = k_{opt}\omega_r^3 + k_{p\_vsg}k_{dc}(\omega_0 - \omega_g) + (\omega_0 - \omega_g)(2H_{vsg}s + D_{vsg}) \quad (14)$$

Simplifying (14) yields:

$$(k_{opt} - k_M)\omega_r^3 + D_{DFIG}\omega_r^2 + (k_{p\_vsg}k_{dc} + D_{vsg})(\omega_0 - \omega_g) + 2H_{vsg}(\frac{d\omega_0}{dt} - \frac{d\omega_g}{dt}) = 0 \quad (15)$$

In steady state, there is $d\omega_0/dt = d\omega_g/dt = 0$, so (15) can be furtherly simplified to

$$\omega_r^3 + \frac{D_{DFIG}}{k_{opt} - k_M}\omega_r^2 + \frac{(k_{p\_vsg}k_{dc} + D_{vsg})}{k_{opt} - k_M}(\omega_0 - \omega_g) = 0 \quad (16)$$

Equation (16) is named stability equation in this paper, the stability analysis of DFIG WTG in $P_0 \sin\delta_{eq} - \omega_r$ plot can be ascribed to this stability equation, which will be analyzed in detail in the next section, this is the mathematical foundation and mechanism of DFIG WTG stability analysis [22].

C. STABILITY PROBLEMS OF VSG-ISynC STRATEGY

1) LIMITED STABILITY BOUNDARY OF VSG-ISynC STRATEGY

Traditional VSG-ISynC control strategy has many disadvantages, the first problem is the limited stability boundary of VSG-ISynC control strategy, especially for frequency drop situation. Given a specific wind speed v_w, if frequency drop is serious enough, then no intersection point can be observed in the $P_0\sin\delta_{eq} - \omega_r$ plot, rotor speed will continue to drop until the entire DFIG WTG system is completely out of control, this is one of the main stability problems for all inertia emulation control strategies including VSG-ISynC strategy.

The stability of VSG-ISynC control strategy can be analyzed through stability equation, the discriminant function Δ of stability function is:

$$\Delta = \left[\frac{D_{DFIG}}{3(k_{opt} - k_M)}\right]^3 + \left[\frac{(k_{p\_vsg}k_{dc} + D_{vsg})(\omega_0 - \omega_g)}{2(k_{opt} - k_M)}\right]^2 \tag{17}$$

The root judgement theory of discriminant function is:

1) $\Delta > 0$, stability function has one real root and a pair of conjugate roots;
2) $\Delta = 0$, stability function has three roots, two of them are identical;
3) $\Delta < 0$, stability function has three different roots.

It is worth mentioning that only the right half of $P_0\sin\delta_{eq} - \omega_r$ plot is shown in this paper, in fact, stability function has its solution which is negative, but the negative solution makes no sense for stability analysis since rotor speed is impossible to be negative. Comparing the root judgement theory to the number of intersections in $P_0\sin\delta_{eq} - \omega_r$ plot, it is easy to find out that the stable situation (two intersections in $P_0\sin\delta_{eq} - \omega_r$ plot) represents the root judgement theory $\Delta < 0$, two roots lie in the right half plan of x-axis, one negative root lies in the left half plan of x-axis, in which case DFIG WTG is able to remain stable after frequency fluctuations. Root judgement theory $\Delta = 0$ represents the situation where the solid line is tangent to the dashed line, two positive roots become identical in this situation, this is also the maximum stability boundary for DFIG WTG, any deeper frequency drop will result in instability. The instability situation refers to $\Delta > 0$ in root judgement theory, one negative real root and a pair of conjugate roots.

2) FREQUENCY SECONDARY DROP OF VSG-ISynC STRATEGY

Speed protection block is usually added into the synchronization loop of VSG- ISynC strategy in order to prevent rotor speed from deep drop. Once rotor speed reaches its minimum limit (0.75pu in this paper), then the function of $P-f$ droop will be immediately disabled, which results in the increase of DFIG rotor speed, it is worth mentioning that the minimum speed limit 0.75 pu is not the critical operating point ω_{rc}, the value of ω_{rc} is unique for a specific wind speed and ω_{rc} is closely related to the DFIG power curve, but the 0.75 pu is the constant minimum value of rotor speed which is allowed to operate for DFIG WTG.

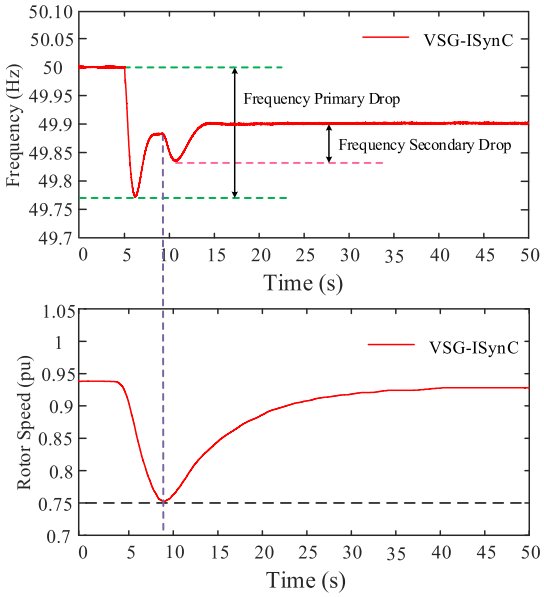

FIGURE 7. Secondary frequency drop for DFIG WTG.

Once the function of $P-f$ droop is disabled, the sudden exit of inertia control will lead to frequency secondary drop due to the serious power unbalance. As is shown in Fig.7, after the initial frequency drop, rotor speed has reached its minimum limit within a short time period, after that, the sudden exit of $P-f$ droop control can significantly lift rotor speed, but will cause serious frequency secondary drop at the same time.

Frequency secondary drop is caused by the change of control topology, but the fundamental reason is that for all inertia emulation control strategies including VSG-ISynC, rotor speed is not considered as a direct control target. If we can add rotor speed control into the regulation of DFIG active power, then VSG-ISynC strategy can achieve the purpose of power regulation and rotor speed regulation at the same time, so that we can prevent rotor speed from decreasing below minimum limit by directly controlling rotor speed.

IV. M-VSG CONTROL STRATEGY FOR DFIG WTG

A. EXPANDED STABILITY BOUNDARY FOR M-VSG CONTROL STRATEGY

The existing VSG-ISynC strategy proposes a serious stability problem for its limited stability boundary, especially for frequency drop situation, rotor speed is likely to be out of control. To address this issue, a modified VSG-ISynC control strategy (M-VSG) is proposed based on the existing VSG-ISynC control strategy, as is shown in Fig.8, M-VSG control strategy modifies the original VSG control strategy by dynamically changing *P-f* droop coefficient k_{p_vsg} according to the change of dc-link voltage, because the dc-link voltage can well reflect the fluctuations of grid frequency under GSC ISynC control strategy.

The equation of droop coefficient k_{p_vsg} can be derived from Fig.8, as is shown below:

$$k_{p\_vsg} = k_{p\_vsg0} - k_{p\_gain}\left(U_{dc}^* - U_{dc}\right) \tag{18}$$

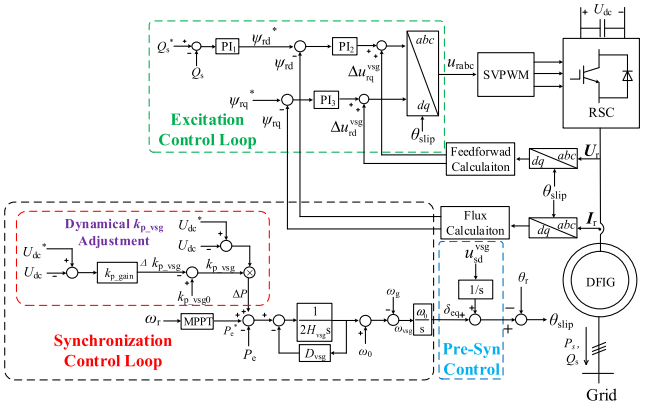

FIGURE 8. M-VSG control strategy to expand stability boundary.

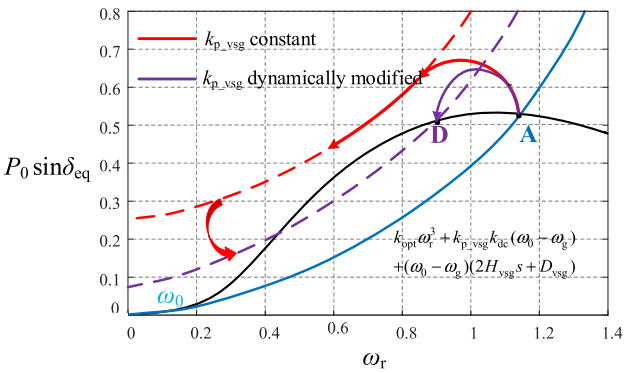

FIGURE 9. Schematic diagram of equilibrium operating point under M-VSG control strategy.

k_{p_vsg0} refers to the value of k_{p_vsg} for traditional VSG control strategy, while k_{p_gain} is the modification coefficient for k_{p_vsg}, so the output of droop control ΔP can be calculated as:

$$\begin{aligned}\Delta P &= \left[k_{p\_vsg0} - k_{p\_gain}\left(U_{dc}^* - U_{dc}\right)\right]\left(U_{dc}^* - U_{dc}\right) \\ &= k_{p\_vsg0}\left(U_{dc}^* - U_{dc}\right) - k_{p\_gain}\left(U_{dc}^* - U_{dc}\right)^2 \end{aligned} \quad (19)$$

For traditional VSG control strategy, *P-f* droop coefficient k_{p_vsg} is considered as a constant value, but in M-VSG control strategy, k_{p_vsg} is an important control subject, which can change its value according to the dc link voltage and improve system stability. During the process of frequency drop, U_{dc} is supposed to be less than U_{dc}^*, which leads to the decrease of k_{p_vsg} as well as ΔP, less extra power is extracted to support power grid, protecting DFIG rotor speed from continuing drop.

The benefit of M-VSG control strategy in frequency drop situation can be seen clearly in the $P_0\sin\delta_{eq} - \omega_r$ plot. As is shown in Fig.9, during the process of serious frequency drop, if k_{p_vsg} remains constant, then there will be no intersection point for DFIG WTG to operate after frequency drop. However, if k_{p_vsg} is dynamically modified during the process according to the trend of grid frequency, then the dashed line in Fig.9 will decrease its value and intersect with the black solid line, as a result, DFIG WTG can still operate under the same level of load increase.

At the same time, for frequency rise situation, as is analyzed in the previous chapter, there will always be the intersection point in $P_0\sin\delta_{eq} - \omega_r$ plot. Moreover, if rotor speed is over 1.2pu, then pitch angle regulator will be activated to control rotor speed around 1.2pu, so that both VSG and M-VSG will not become out of control in frequency rise situation. There are still some advantages for M-VSG control strategy in frequency rise situation. U_{dc} is supposed to be greater than U_{dc}^* when frequency rises, so the signal of $k_{p\_vsg0}(U_{dc}^*$- $U_{dc})$ in (19) is negative, consequently, the absolute value of ΔP is greater than traditional VSG control strategy with only k_{p_vsg0} $(U_{dc}^*$- $U_{dc})$ in its droop control loop, which means that, there exists a greater power unbalance for M-VSG control strategy in its synchronization control loop, it is beneficial to make the rotor speed increase faster to absorb the active power more quickly, so that the degree of frequency rise can be well damped with M-VSG control strategy. It is worth mentioning that, although M-VSG control strategy is beneficial for frequency rise situation, considering the fact that no matter how serious the frequency rise is, DFIG will not oscillate in this situation and the advantage of frequency damping ability is not so obvious and necessary, so this paper is mainly focused on the stability analysis under frequency drop situation.

The reason why the signal of dc-link voltage, which reflects the change of grid frequency, is chosen to modify k_{p_vsg} is that during the initial time period when frequency changes, the deviation of equilibrium operating point is the most serious, k_{p_vsg} need to change quickly enough so as to avoid losing synchronization, while the change of grid frequency is also the most obvious during the same time period, so that the signal of grid frequency can meet the requirement of k_{p_vsg} modification. Additionally, since GSC ISynC control strategy can transfer the change of grid frequency to the change of dc-link voltage, the measurement of dc-link voltage is more economical than the complicated frequency detection devices. Based on the analysis above, the signal of dc-link voltage is finally selected to dynamically change *P-f* droop coefficient k_{p_vsg}.

When it comes to the droop coefficient k_{p_vsg}, the modification of k_{p_vsg} should satisfy the minimum requirement of stability. According to the stability analysis in the resubmitted manuscript, the stable operation of DFIG WTG means the discriminant function $\Delta < 0$:

$$\left[\frac{D_{DFIG}}{3(k_{opt} - k_M)}\right]^3 + \left[\frac{(k_{p\_vsg}k_{dc} + D_{vsg})(\omega_0 - \omega_g)}{2(k_{opt} - k_M)}\right]^2 < 0 \quad (20)$$

So that we can get the function between droop coefficient k_{p_vsg} and the frequency deviation $\omega_0 - \omega_g$ by simplifying (20):

$$(k_{p\_vsg}k_{dc} + D_{vsg})(\omega_0 - \omega_g) < \frac{2 \times 3^{-\frac{3}{2}} \times D_{DFIG}^{\frac{3}{2}}}{\sqrt{k_M - k_{opt}}} \quad (21)$$

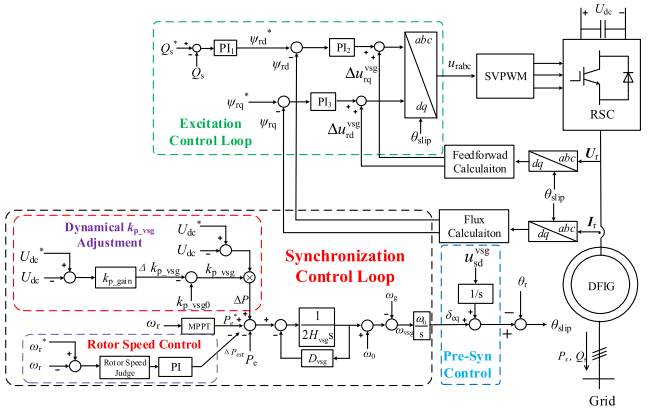

FIGURE 10. Rotor speed regulation of M-VSG control strategy.

For frequency drop situation, $(\omega_0 - \omega_g) > 0$, so the droop coefficient k_{p_vsg} should satisfy the following equation:

$$0 < k_{p\_vsg} < \frac{2 \times 3^{-\frac{3}{2}}}{(\omega_0 - \omega_g)k_{dc}} \times \frac{D_{DFIG}^{\frac{3}{2}}}{\sqrt{k_M - k_{opt}}} - \frac{D_{vsg}}{k_{dc}} \quad (22)$$

For frequency rise situation, $(\omega_0 - \omega_g) < 0$, the modification of k_{p_vsg} will always satisfy (21), this is consistent with the conclusion that there will always be the intersection point in $P_0 \sin\delta_{eq} - \omega_r$ plot for frequency rise situation, both VSG and M-VSG will not become oscillating and out of control.

B. ROTOR SPEED CONTROL FOR M-VSG CONTROL STRATEGY

Frequency secondary drop is caused by the sudden exit of $P-f$ droop control, but the fundamental reason is that DFIG rotor speed is not under control during the process of inertia response. If we can control rotor speed to keep it constant at the minimum value once reaching this lowest limit, then the serious frequency secondary drop can be avoided. In order to realize rotor speed control for DFIG WTG while preserving the function of inertia response and frequency regulation, an additional rotor speed control loop is added in the existing VSG synchronization control loop, rotor speed control loop can only be activated when rotor speed has decreased below minimum speed. Detailed control diagram of M-VSG control strategy to avoid frequency secondary drop is illustrated in Fig.10, it is worth mentioning that rotor speed control loop is added based on the M-VSG control strategy which can dynamically change the value of k_{p_vsg}.

For VSG-ISynC control strategy, the control of DFIG active power is accomplished through the regulation of equivalent power angle δ_{eq}. Similarly, DFIG rotor speed control is also achieved through the control of δ_{eq}. Once rotor speed has decreased below the permitted minimum speed, then the control block of rotor speed judge will be activated to enable rotor speed PI regulator, the regulation of DFIG rotor speed will generate an additional power output $\Delta P_{\omega r}$, then $\Delta P_{\omega r}$ is able to change the value of equivalent power angle δ_{eq} in synchronization control loop, which results in the power

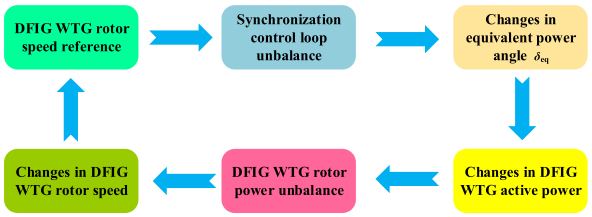

FIGURE 11. Control flow chart of M-VSG rotor speed regulation.

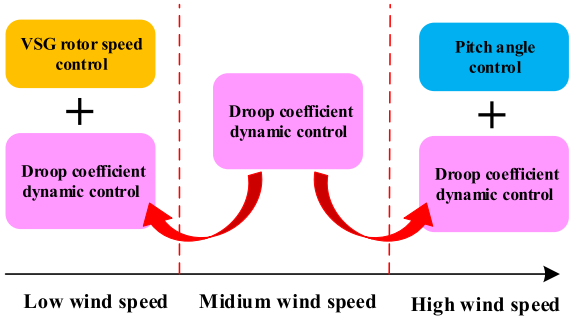

FIGURE 12. Systematic M-VSG control strategy from low wind speed to high wind speed.

unbalance for DFIG wind turbine. Finally, the power unbalance will change DFIG rotor speed, since a PI regulator is used in the rotor speed control loop, the rotor speed dynamic process will not stop until the feedback of rotor speed equals the input rotor speed reference. The control flow chart is illustrated in Fig.11, which includes a closed loop from rotor speed reference, to equivalent power angle δ_{eq} and finally return to rotor speed feedback.

C. SYSTEMATIC CONTROL STRATEGY OF M-VSG FOR DFIG WTG

According to the two modifications proposed above, a systematic control strategy for DFIG WTG is shown in Fig.12. M-VSG control strategy will replace the original VSG control strategy to expand stability boundary from low wind speed to high wind speed. Moreover, when rotor speed is expected to decrease lower than permitted minimum limit in low wind speed situation, then an additional rotor speed control loop will be activated to prevent rotor speed from continuing drop. At the same time, when rotor speed is going to increase over upper limit, the pitch angle controller will be enabled to decrease rotor speed. Compared with the conventional VSG control strategy, the proposed M-VSG control strategy has its obvious advantage in expanding stability boundary as well as in avoiding undesired frequency secondary drop.

V. STABILITY ANALYSIS OF M-VSG CONTROL STRATEGY

A. QUANTITATIVE ANALYSIS OF STABILTY MARGIN AND COEFFICIENT KP_VSG

The mathematical foundation of $P_0 \sin\delta_{eq} - \omega_r$ plot is a cubic function with ω_r as the only variable, the most extreme situation that DFIG WTG can still remain stable operation

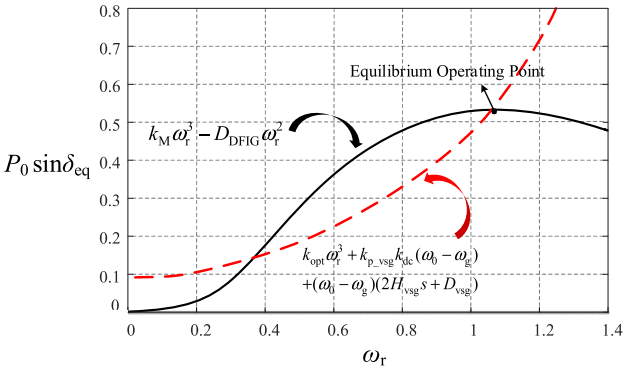

FIGURE 13. Description of stability margin for VSG-ISynC strategy.

is when discriminant function Δ equals to zero, which means the power curve of (7) and (13) are tangent to each other, as is shown below

$$\Delta = \left[\frac{D_{DFIG}}{3(k_{opt} - k_M)}\right]^3 + \left[\frac{(k_{p\_vsg}k_{dc} + D_{vsg})(\omega_0 - \omega_g)}{2(k_{opt} - k_M)}\right]^2 = 0 \tag{23}$$

Equation (23) shows the direct relation between the grid frequency drop $\omega_0 - \omega_g$ and important control parameters in VSG-ISynC control strategy under the most extreme condition, the maximum grid frequency drop $\Delta\omega_{gmax}$ can be calculated from (23) as

$$\Delta\omega_{g\,max} = \omega_0 - \omega_g = \sqrt{\frac{4D_{DFIG}^3(k_{opt} - k_M)^2}{27(k_M - k_{opt})^3(k_{p\_vsg}k_{dc} + D_{vsg})^2}} \tag{24}$$

The direct relation between $\Delta\omega_{gmax}$ and *P-f* droop coefficient k_{p_vsg} is described in (24), for traditional VSG-ISynC control strategy, k_{p_vsg} is considered as a constant value, so the $\Delta\omega_{gmax}$ is constant given with a specific wind speed and other important control parameters. However, in M-VSG control strategy, the k_{p_vsg} is dynamically modified according to the fluctuation of dc link voltage, because dc link voltage is strictly synchronized with grid frequency fluctuation under GSC ISynC control strategy, in which case when grid frequency drops, k_{p_vsg} will also lower its value, this is decisive in increasing the maximum grid frequency drop that DFIG WTG can tolerate.

Moreover, we use the definition of stability margin, which is introduced in [22], to help us better understand the influence of k_{p_vsg} in expanding $\Delta\omega_{gmax}$ in a more direct and visualized way. In Fig.5, the black solid line and the red dashed line stand for the equation of (13) and (7) respectively, the overlapping area between (13) and (7) is defined as the stability margin, as is shown in Fig.13, the area which is filled with blue dashed line is stability margin.

Since the stability margin is the overlapping area between (7) and (13), the larger the stability margin is, the deeper frequency drop DFIG WTG can tolerate, if stability margin becomes zero due to frequency drop, then the DFIG WTG will run at the critical operation point. The mathematical expression of stability margin S_{sm} is obtained as

$$\begin{aligned} S_{sm} = &\int_{\omega r1}^{\omega r2} \Big[(k_M - k_{opt})\omega_r^3 - D_{DFIG}\omega_r^2 \\ &- (k_{p\_vsg}k_{dc} + D_{vsg})(\omega_0 - \omega_g)\Big]d\omega_r \\ &- 2H_{vsg}\int_{\omega r1}^{\omega r2}\left(\frac{d\omega_0}{dt} - \frac{d\omega_g}{dt}\right)d\omega_r \end{aligned} \tag{25}$$

ω_{r1} and ω_{r2} refer to the two intersection points between power curves of (7) and (13), during the dynamic process of frequency drop, $d\omega_0/dt = 0$, so the final expression of stability boundary is obtained as

$$\begin{aligned} S_{sm} = &\frac{k_M - k_{opt}}{4}(\omega_{r2}^4 - \omega_{r1}^4) - \frac{D_{DFIG}}{3}(\omega_{r2}^3 - \omega_{r1}^3) \\ &- \left[(k_{p\_vsg}k_{dc} + D_{vsg})(\omega_0 - \omega_g) + 2H_{vsg}\frac{d\omega_g}{dt}\right](\omega_{r2} - \omega_{r1}) \end{aligned} \tag{26}$$

The advantage of M-VSG control strategy to dynamically modify k_{p_vsg} can be seen obviously in expanding the stability margin, the area of stability margin will increase if k_{p_vsg} decreases its value according to dc link voltage, which denotes that DFIG WTG can still operate stably under a deeper level frequency drop where traditional VSG-ISynC control strategy cannot tolerate.

B. STATE SPACE MODELING AND STABILITY ANALYSIS OF M-VSG CONTROL STRATEGY

With the introduction of dynamically modified k_{p_vsg} during the process of inertia response, DFIG WTG is able to increase its stability margin, the mechanism and quantitative analysis is explained in the previous section. In this section, further analysis is conducted based on the state space modelling of M-VSG control strategy.

The output active power of DFIG WTG is shown as followed

$$P_e = \frac{E_r^{eq}U_s}{X_{eq}}\sin\delta_{eq} = P_0\sin\delta_{eq} \tag{27}$$

where E_r^{eq} is DFIG equivalent electromotive force, U_s is DFIG stator voltage, X_{eq} refers to the equivalent reactance between DFIG and power grid.

linearizing (27) around its steady state operation point yields:

$$\begin{aligned} \Delta P_e = &\frac{E_{r0}^{eq}U_{s0}}{X_{eq}}\cos\delta_{eq0}\Delta\delta_{eq} + \frac{E_{r0}^{eq}\sin\delta_{eq0}}{X_{eq}}\Delta U_s \\ &+ \frac{U_{s0}\sin\delta_{eq0}}{X_{eq}}\Delta E_r^{eq} \\ = &k_{P\delta}\Delta\delta_{eq} + k_{PU}\Delta U_s + k_{PE}\Delta E_r^{eq} \end{aligned} \tag{28}$$

E_{r0}^{eq}, δ_{eq0} and U_{s0} are the steady state value of E_r^{eq}, δ_{eq} and U_s respectively. During the process of frequency fluctuation and inertia response, the variation of DFIG stator voltage ΔU_s and equivalent electromotive force $\Delta \boldsymbol{E}_r^{eq}$ can be neglected,

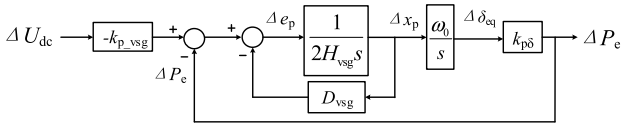

FIGURE 14. Small-signal diagram of VSG active power control loop.

so ΔP_e is only proportional to $\Delta\delta_{eq}$ in this situation. Neglecting the variation of rotor speed, then the small-signal control diagram of active power control loop of VSG control strategy is shown in Fig.14, all variables have all been transformed into per-unit values.

In Fig.14, the input variable Δe_p can be calculated according to the following equation:

$$\Delta e_p = -k_{p\_vsg}\Delta U_{dc} - D_{vsg}\Delta x_p - k_{p\delta}\Delta\delta_{eq} \tag{29}$$

Besides, the relation between the input Δe_p and the output Δx_p is given by:

$$\Delta x_p = \Delta e_p \frac{1}{2H_{vsg}s} \tag{30}$$

Subsuming (29) into (30) yields the state equation about the output variable Δx_p:

$$\frac{d\Delta x_p}{dt} = \frac{-k_{p\_vsg}}{2H_{vsg}}\Delta U_{dc} - \frac{D_{vsg}}{2H_{vsg}}\Delta x_p - \frac{k_{p\delta}}{2H_{vsg}}\Delta\delta_{eq} \tag{31}$$

Similarly, the state equation about the output variable $\Delta\delta_{eq}$ is

$$\frac{d\Delta\delta_{eq}}{dt} = \omega_0\Delta x_p \tag{32}$$

For GSC ISynC control strategy, the space state model is obtained by linearizing it around the steady operation point, as is introduced in reference [16]. Because the phase angle of GSC output voltage δ_g is the output of integrator, so the output voltage of GSC in d-axis and q-axis are:

$$U_{gd} = U_{td}^* U_{dc} \tag{33}$$
$$U_{gq} = U_{tq}^* U_{dc} \tag{34}$$

where U_{td}^* and U_{tq}^* are the GSC modulation voltage U_t in d-axis and q-axis in per-unit value. So the linearization of (33) and (34) are obtained as

$$\Delta U_{gd} = U_{dc0}\Delta U_{td}^* + U_{td0}^*\Delta U_{dc} \tag{35}$$
$$\Delta U_{gq} = U_{dc0}\Delta U_{tq}^* + U_{tq0}^*\Delta U_{dc} \tag{36}$$

U_{dc0}, U_{td0}^* and U_{tq0}^* are the steady state value of U_{dc}, U_{td}^* and $U_{tq.}^*$ Because the modulation voltage is oriented at d-axis, and the phase angle of GSC output voltage δ_g is relatively small, then the relation among U_t, ΔU_{td}^* and ΔU_{tq}^* can be described by the following equations:

$$U_{td0}^* = U_g \tag{37}$$
$$U_{tq0}^* = 0 \tag{38}$$
$$\Delta U_{td}^* = 0 \tag{39}$$
$$\Delta U_{tq}^* = U_g \sin(\Delta\delta_g) \approx U_g\Delta\delta_g \tag{40}$$

Substituting (37)-(40) to (35) and (36), we get:

$$\Delta U_{gd} = U_g\Delta U_{dc} \tag{41}$$
$$\Delta U_{gq} = U_{dc0}U_g\Delta\delta_g \tag{42}$$

The linearization of GSC active power is:

$$\Delta P_g = U_{gd}\Delta I_{gd} + U_{gq}\Delta I_{gq} + I_{gd}\Delta U_{gd} + I_{gq}\Delta U_{gq} \tag{43}$$

where U_{gd} and U_{gq} are the GSC output voltage in d-axis and q-axis, I_{gd} and I_{gq} are the output current in d-axis and q-axis respectively.

The linearization of dc link voltage differential equation for DFIG WTG is derived from (1), as is shown below.

$$2H_C\frac{d\Delta U_{dc}}{dt} = \frac{s_{slip}}{s_{slip}-1}\Delta P_e - \Delta P_g \tag{44}$$

where s_{slip} is the slip angular velocity of DFIG WTG, considering that GSC output voltage U_g is oriented at d-axis, so U_{gq} is zero, then the space state equation of ΔU_{dc} is obtained by substituting (28) (41) (42) (43) into (44), which is:

$$\frac{d\Delta U_{dc}}{dt} = -\frac{I_{gd}U_g}{2H_C}\Delta U_{dc} - \frac{U_{dc0}I_{gq}U_g}{2H_C}\Delta\delta_g - \frac{U_{gd}}{2H_C}\Delta I_{gd} + \frac{s_{slip}k_{p\delta}}{2H_C\left(s_{slip}-1\right)}\Delta\delta_{eq} \tag{45}$$

At the same time, the space state equation about the small signal $\Delta\delta_g$ satisfies the following equation:

$$\frac{d\Delta\delta_g}{dt} = \omega_0\Delta U_{dc} \tag{46}$$

The differential equation of GSC output current in d-axis and q-axis are given by:

$$\frac{d\Delta I_{gd}}{dt} = \frac{\omega_0 U_g}{L_g}\Delta U_{dc} - \frac{\omega_0 R_g}{L_g}\Delta I_{gd} + \omega_0\Delta I_{gq} \tag{47}$$
$$\frac{d\Delta I_{gq}}{dt} = \frac{\omega_0 U_g}{L_g}\Delta\delta_g - \omega_0\Delta I_{gd} - \frac{\omega_0 R_g}{L_g}\Delta I_{gq} \tag{48}$$

L_g and R_g are the grid inductance and resistance, ω_0 is the rated grid angular frequency. The state space model for M-VSG control strategy is built on the following state space variables:

$$\Delta x = [\Delta x_p\ \Delta\delta_{eq}\ \Delta U_{dc}\ \Delta\delta_g\ \Delta I_{gd}\ \Delta I_{gq}]^T \tag{49}$$

The eigen equation for M-VSG control strategy is finally obtained based on (31), (32), (45), (46), (47), (48):

$$\frac{d\Delta x}{dt} = A\Delta x \tag{50}$$

A is the 6-order eigen matrix of M-VSG control strategy. The eigenvalues of M-VSG control strategy can be calculated through the following equation:

$$\det(\lambda I - A) = 0 \tag{51}$$

$\boldsymbol{I}$ represents the 6×6 identity matrix. The stability analysis is carried out based on 2MW DFIG WTG, all important electrical parameters, aerodynamic parameters as well as control parameters are listed in Table 1.

TABLE 1. Main parameters of 2MW DFIG WTG.

Main Electrical Parameters		
Symbol	Parameter	Value
U_{sB}	Rated Stator Voltage L-L /kV	0.69
U_g	Grid Voltage/kV	0.69
TR	Turn Ratio /pu	0.333
S_B	Rated Power /MWA	2
f_N	Rated Frequency /Hz	50
ω_0	Base value of grid angular frequency/rad/s	314
C	Dc Link Capacitance/mF	3.6
R_s	Stator Resistance/pu	0.0344
L_{ls}	Stator Leakage Reactance/pu	0.2748
L_m	Magnetizing Reactance/pu	12.97
R_r	Rotor Resistance/pu	0.0273
L_{rs}	Rotor Leakage Reactance /pu	0.3979
H_C	Capacitance Inertia Time Constant/ms	3.8
L_g	Grid Inductance/pu	0.1
R_g	Grid Resistance/pu	0.005
Main Aerodynamic Parameters		
Symbol	Parameter	Value
$S_{Turbine}$	Rated Turbine Power/MW	2.18
$v_{w\_cut\text{-}in}$	Cut-in Wind Speed/m/s	3
v_{w_rated}	Rated Wind Speed/m/s	11.8
$v_{w\_cut\text{-}out}$	Cut-out Wind Speed/m/s	25
D	Turbine Diameter /m	90.76
λ_{opt}	Optimal Tip-speed Ratio	8.37δg
C_{pmax}	Optimal Power Coefficient	0.483
Main control parameters of M-VSG control strategy		
Symbol	Parameter	Value
D_{vsg}	VSG Damping factor	200
H_{vsg}	VSG rotor Inertia Time Constant/s	15
$k_{p\psi r}$	Proportional Gain of ψ_r Controller	2
$k_{i\psi r}$	Integral Gain of ψ_r Controller	0.032

P-f droop coefficient k_{p_vsg} is a decisive parameter in determining the stability of DFIG WTG under M-VSG control strategy, Fig.15 shows the loci of system eigenvalues as the function of k_{p_vsg}, with the increase of k_{p_vsg} from 1 to 50, pole No.1 move away from the real axis to imaginary axis until moving into the right half plane, which directly decreases the system damping ratio and leads to system instability, pole No.2 shows the similar trend of moving from left half plane to the right half plane. Other poles are all located far away from imaginary axis in the left half plane, which will not have adverse impact on system stability. For M-VSG control strategy, because it is able to change the value of k_{p_vsg} according to dc link voltage and grid frequency, so M-VSG control strategy is able to drag back system poles back within the stable left half plane even under severe frequency drop situations.

In this chapter, detailed stability analysis is conducted for M-VSG control strategy, quantitative indexes of maximum

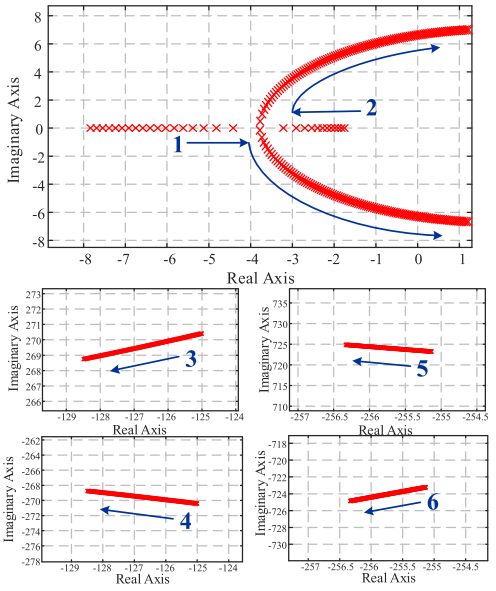

FIGURE 15. Loci of system eigenvalues as the function of k_{p_vsg}.

grid frequency drop $\Delta\omega_{gmax}$ and stability margin is derived as the function of *P-f* droop coefficient k_{p_vsg}, afterwards, the state space equation of M-VSG control strategy is built to get the loci of system eigenvalues as a function of k_{p_vsg}, both the quantitative stability analysis and space state equation demonstrate that M-VSG control strategy, which can dynamically change the value of k_{p_vsg}, is able to increase system stability boundary. Experiment verification will be conducted in the next two chapters to show the control performance of M-VSG control strategy in time-domain situation.

VI. RESEARCH PLATFORM FOR DFIG INERTIA EMULATION CONTROL

In order to verify the effectiveness of proposed M-VSG control strategy, both simulations and hardware-in-loop (HIL) experiments are conducted in co-simulation research platform. As is shown in Fig 13, co-simulation research platform needs 4 upper computers working together to guarantee real-time simulation. All electrical parts are built in Real-Time Digital Simulator (RTDS) in upper computer #1, including DFIG model, back-to-back converter model and power grid model. All aerodynamics model of DFIG WTG is built in GH Bladed in upper computer #3, such as 3D wind model, structural dynamics model and pitch actuators model. Upper computer #2 is in charge of loading controlling file to DSP controller and monitoring its operation condition, while upper computer #4 is used as the interface of main control programmable logic controller (PLC).

As is shown in Fig.16, co-simulation research platform includes a real-time communication system between RTDS and GH Bladed, and a HIL communication system between RTDS and hardware DSP controller. The key issue of co-simulation platform is the interface communication because simulation time step for GH Bladed is around 10ms while

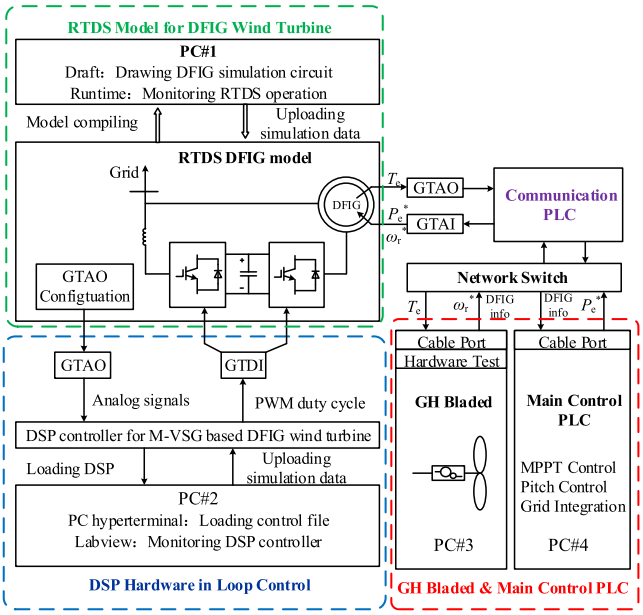

FIGURE 16. Schematic diagram of co-simulation research platform.

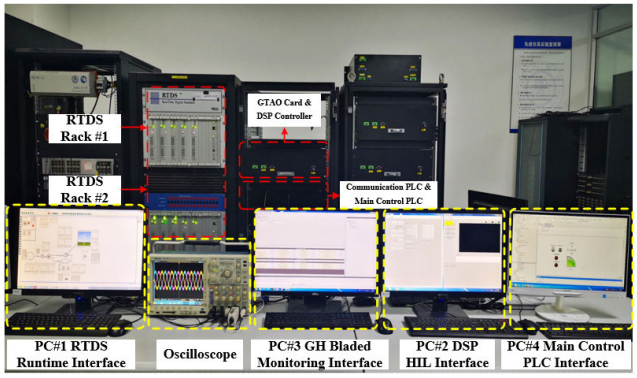

FIGURE 17. Co-simulation research platform.

that for RTDS are 50μs for power system model and 2μs for power electronics model. To solve this problem, a PLC is used as the communication interface, at the same time, a special module called Hardware Test is inserted into GH Bladed to guarantee real-time two-way communication. As is shown in Fig.16 and Fig.18, DFIG electromagnetic torque signal T_e is firstly transmitted from RTDS to communication PLC via RTDS Gigabit Transceiver Analogue Output Card (GTAO Card), and is then delivered to GH Bladed software through network switch. GH Bladed software then calculates DFIG rotor speed reference ω_r^* based on the received T_e signal. Similar to the transmit route of T_e, ω_r^* is transmitted to communication PLC through network switch and is then fed back to RTDS by Gigabit Transceiver Analogue Input Card (GTAI Card), so that a communication signal closed loop is completed with T_e as RTDS output and ω_r^* as input.

Moreover, main control PLC is responsible for MPPT control, pitch control as well as grid integration, it collects DFIG WTG information from GH Bladed and generates power reference P_e^* for DFIG WTG, P_e^* is sent to RTDS together with ω_r^* via communication PLC and GTAI.

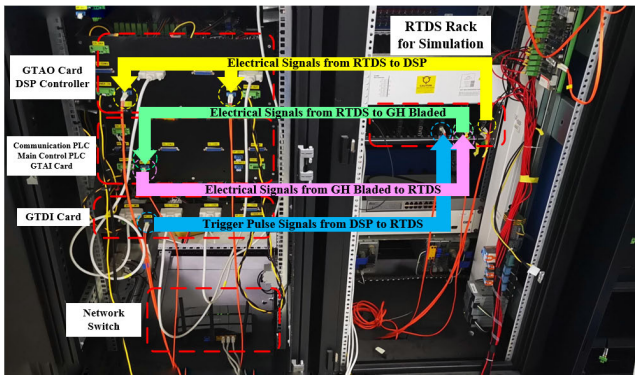

FIGURE 18. Signal Transmit Route of Co-simulation Research Platform.

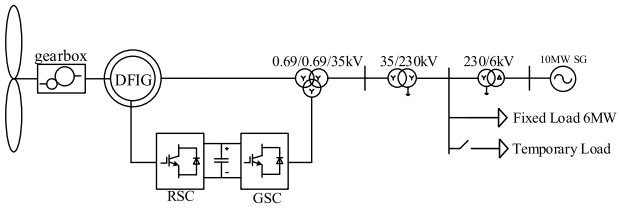

FIGURE 19. Experiment topology for M-VSG control strategy.

RTDS HIL is able to conduct complex power system experiments to verify the feasibility of different control strategies in real DSP controller. In this paper, hardware DSP controller adopts OMAP-L137 as its processor, FPGA and CPLD are also used as auxiliary processor resources. All electrical parts of DFIG WTG are built in RTDS while DFIG M-VSG converter control strategy is embedded in DSP controller. Necessary electrical signals are transmitted to DSP controller for calculation through GTAO Card, then DSP controller will send DFIG converter trigger pulse signals back to RTDS through Gigabit Transceiver Digital Input Card (GTDI Card), so that a HIL signal closed loop is completed with electrical signals as RTDS output and converter trigger pulse signals as input.

In this paper, the experiment topology is developed based on one machine system, as is shown in Fig.19, a 2MW DFIG wind turbine is connected to power grid which is emulated by a 10MW SG. A load change is realized by adding temporary load so that it provokes fluctuations in power grid frequency. Detailed electrical and aerodynamic parameter is listed in Table 1.

VII. EXPERIMENT VERIFICAITON OF M-VSG CONTROL STRATEGY

A. SIMULATION AND COMPARISON RESULTS OF DFIG INERTIA RESPONSE

As is analyzed in Chapter V, M-VSG has its obvious advantages in expanding stability boundary. In order to verify the control performance of M-VSG control strategy, a relatively larger temporary load (2.5MW) is added into power system at $t = 2$s, which will cause a more severe power fluctuation.

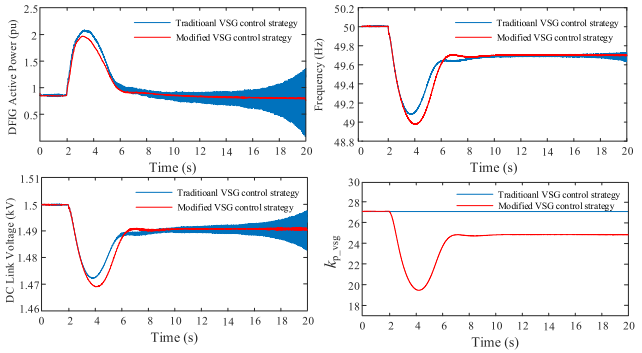

FIGURE 20. DFIG inertia response in frequency drop situation.

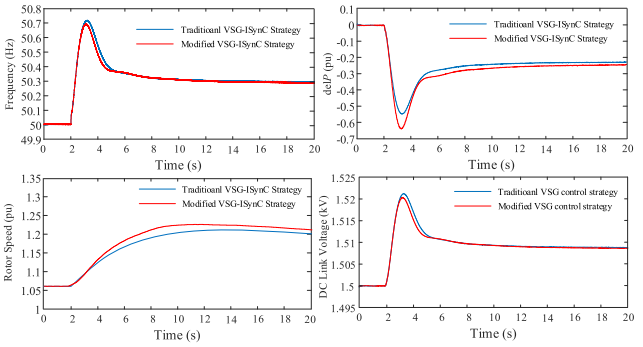

FIGURE 21. DFIG inertia response in frequency rise situation.

Simulation results are shown in Fig.20, for traditional VSG control strategy, after a short-time active power rise to support power gird, DFIG WTG cannot remain stable, an obvious power oscillation is observed especially after $t = 6$s, which means that DFIG WTG cannot find its new equilibrium operating point after load change. However, if VSG is replaced by M-VSG control strategy, then it is easy to find out that DFIG active power can still keep stable, because the signal of dc link voltage is used to dynamically change VSG droop coefficient $k_{\mathrm{p\_vsg}}$, which controls the equilibrium operating point within an acceptable range.

Similar control results can also be found in the plot of grid frequency as well as dc link voltage. Since DFIG active power is eventually unstable after the load change of 2.5MW, all related electrical signals are affected by the oscillations of active power.

For M-VSG control strategy, as is shown in Fig.20, the droop coefficient $k_{\mathrm{p\_vsg}}$ is less than that of traditional VSG control strategy during the same process of transient inertia response, especially for the initial several seconds after frequency drop, the decrease of $k_{\mathrm{p\_vsg}}$ is more significant to force DFIG WTG to return back to stable region. The additional power support of M-VSG is also less than traditional VSG control strategy, which results in the fact that the minimum grid frequency of M-VSG control strategy is obviously lower than traditional VSG control strategy. It seems that the grid frequency damping performance of VSG control strategy is better than M-VSG control strategy, but VSG cannot remain stable after severe load change. So a better frequency damping performance and a wider DFIG stability boundary are two contradictory issues and we cannot achieve both of them at the same time. To some extent, M-VSG control strategy is able to expand the stability boundary at the sacrifice of losing its grid frequency damping ability, but this sacrifice is necessary because the consequences of power oscillation is more severe than deeper frequency drop.

On the other hand, if 2.5MW load is thrown off from power grid, it will cause a serious frequency rise, however, because there will always be intersection point in $P_0\sin\delta_{\mathrm{eq}} - \omega_{\mathrm{r}}$ plot, so DFIG WTG will not become out of control like frequency drop situation. As is shown in Fig.21, during the process of frequency rise, the absolute value of ΔP for M-VSG control strategy is obviously greater than traditional VSG control strategy, so the DFIG rotor speed will increase faster to absorb more active power, the degree of frequency rise can be well damped, which is beneficial to the stable operation of the entire power grid.

B. SIMULATION AND COMPARISON RESULTS OF GRID FREQUENCY SECONDARY DROP

Another obvious advantage of M-VSG control strategy is its direct control of DFIG rotor speed when rotor speed has decreased lower than the permitted minimum value. This function is verified through the co-simulation research platform, detailed comparison between traditional VSG control strategy and M-VSG control strategy in terms of frequency secondary drop is shown in Fig.22. Grid frequency remains stable at 50Hz before extra load is added into power system and rotor speed is around 0.92pu. The first transient of primary frequency drop for both traditional VSG and M-VSG strategy is similar to each other, they all experience the same level of frequency drop as well as the decrease of DFIG rotor speed.

Major difference lies in the response when rotor speed has reached the minimum rotor speed. For traditional VSG control strategy, once rotor has reached the minimum value, then the function of rotor speed protection will be activated by disabling the *P-f* droop control, so the sudden power unbalance will lead to the rise of DFIG rotor speed and an obvious frequency secondary drop, which will impose an adverse impact on power grid stability.

However, for M-VSG control strategy proposed in this paper, the regulation of DFIG rotor speed will be enabled instead of the sudden exit of *P-f* droop control upon reaching the minimum rotor speed. As a result, it can be seen from Fig.22 that the additional power output $\Delta P_{\omega\mathrm{r}}$ will increase, which has a decisive effect on the equivalent power angle δ_{eq} through the rotor swing equation, so DFIG rotor speed can quickly return back and remain stable around the speed reference. At the same time, the undesired frequency secondary drop can also be avoided due to the direct control of DFIG rotor speed, which is beneficial to the stable operation of DFIG WTG.

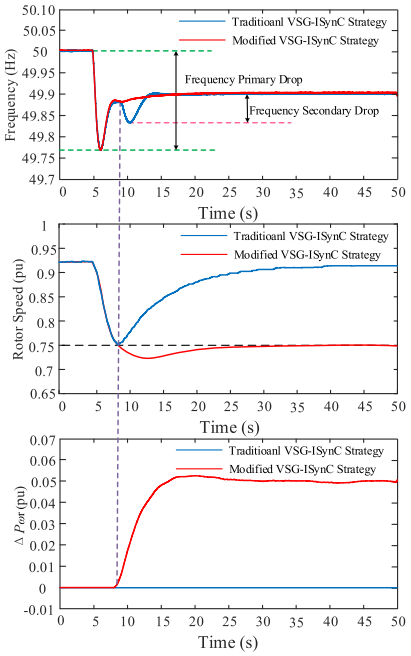

FIGURE 22. Rotor speed control of M-VSG control strategy.

C. SIMULATION RESULTS IN HIGH WIND SPEED

A systematic control strategy for DFIG WTG is proposed in this paper, simulation results of dynamic response in low wind speed and medium wind speed have already been shown in the previous two sections. In this section, simulation results will be shown in terms of high wind speed situation.

When DFIG WTG is operating in high wind speed situation, then the pitch angle regulation will be enabled once rotor speed has exceeded the permitted highest speed to protect wind turbine. Fig.23 shows the dynamic response of DFIG WTG in a turbulent wind speed situation, this aerodynamic simulation is completed in GH Bladed software, where the mean wind speed is 11m/s, and the longitudinal, lateral and vertical percentage of turbulence intensity are 14.3038%, 11.2646% and 8.0872% respectively.

From Fig.23 it can be observed that the pitch angle regulator will function timely and quickly to change the wind turbine pitch angle according to DFIG rotor speed, aiming to stabilize the rotor speed within a relatively small margin around 1.2 pu. It is one of the main function of pitch angle regulator, another important function is that when a part of system load is going to be thrown off from power gird, the power unbalance will cause the rise of rotor speed until reaching a new steady state. In high wind speed situation, rotor speed is likely to increase over 1.2pu, where pitch angle regulator will then be activated to prevent over-speed. As is shown in Fig.24, 1MW load is thrown off from power system at $t = 5$s, rotor speed will increase to nearly 1.25pu if pitch angle regulation is disabled, however, if pitch angle regulation is enabled, then pitch angle will increase accordingly to keep rotor speed stable at 1.2 pu.

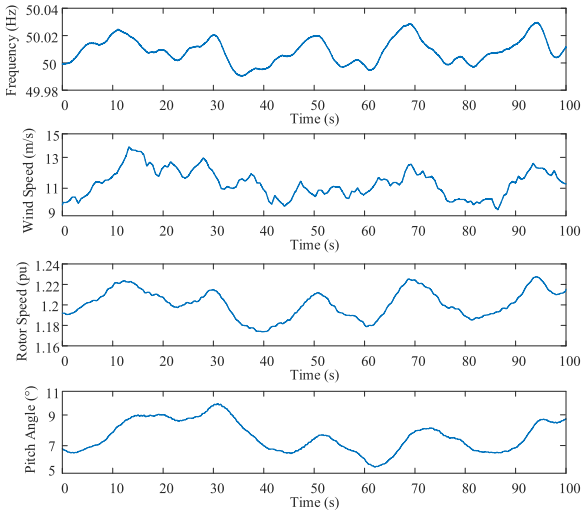

FIGURE 23. Dynamic response of DFIG pitch angle regulator under turbulent wind.

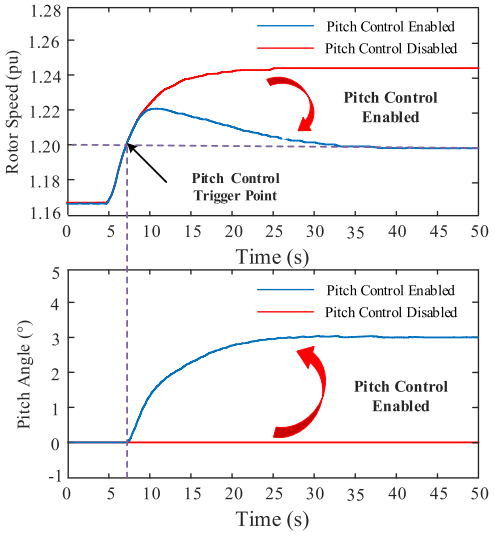

FIGURE 24. Dynamic response of DFIG pitch angle regulator under load-off situation.

D. EXPERIMENT RESULTS OF RTDS HIL VERIFICATION

Co-simulation research platform is able to conduct HIL experiments to test the feasibility of proposed M-VSG control strategy in hardware DSP controller. Among all important electrical signals transmitted between RTDS and GH Bladed, rotor current and PCC voltage/current are selected to compare the control performance of different control strategies, detailed waveforms are plotted in oscilloscope, as is shown from Fig.25 to Fig.29.

DFIG rotor current comparison is shown in Fig.25, under traditional VSG control strategy, when 2.5MW temporary load is added into power system, rotor current experiences a short period of rise-and-fall process, after that, for traditional VSG control strategy, rotor current gradually becomes oscillating, indicating that DFIG WTG cannot return back to its

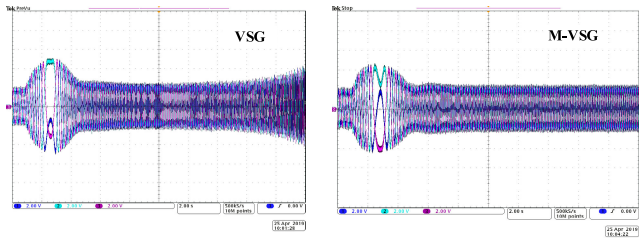

FIGURE 25. Rotor current comparison between VSG and M-VSG.

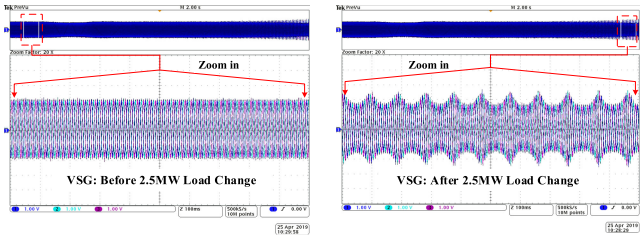

FIGURE 26. PCC voltage of DFIG WTG under VSG control strategy.

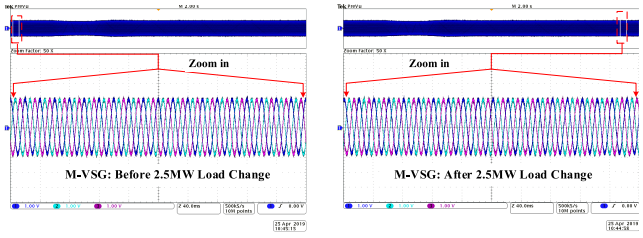

FIGURE 27. PCC voltage of DFIG WTG under M-VSG control strategy.

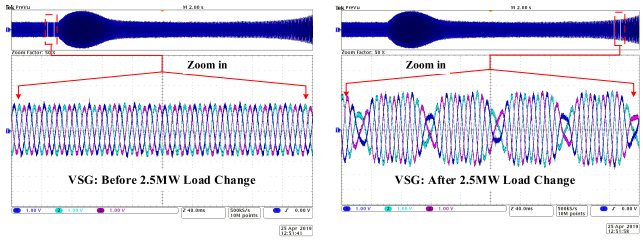

FIGURE 28. PCC current of DFIG WTG under VSG control strategy.

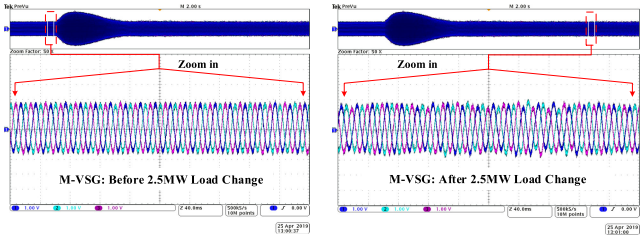

FIGURE 29. PCC current of DFIG WTG under M-VSG control strategy.

original stable region, but M-VSG control strategy can keep stable in the same scenario.

PCC voltage and PCC current are another two important electrical signals to show the stability of different control strategies. Considering that the entire transient inertia response will last for almost 20 seconds and it is not convenient to plot the whole process in oscilloscope for detailed comparison, so we select and amplify the waveform of a short

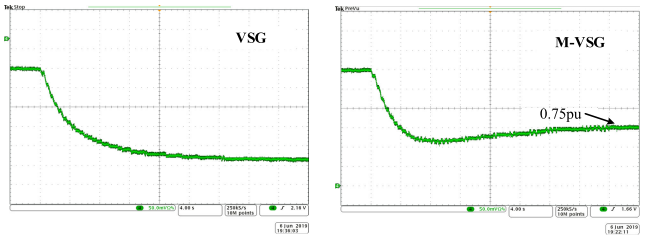

FIGURE 30. DFIG rotor speed comparison between VSG and M-VSG (low wind speed).

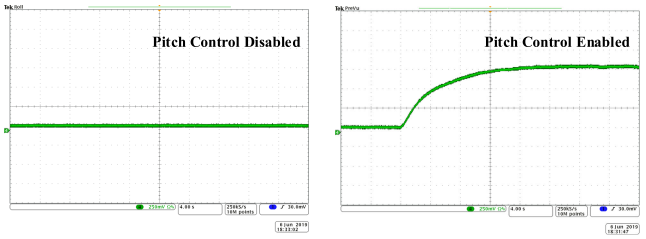

FIGURE 31. DFIG pitch angle comparisons in load-off situation.

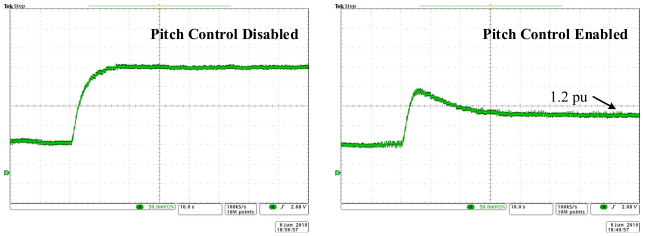

FIGURE 32. DFIG rotor speed comparison in load-off situation.

time period before 2.5MW load change and after 2.5MW load change, as is shown from Fig.26-Fig.29. Experiment results of PCC voltage and current are similar to that of DFIG rotor current. For traditional VSG control strategy, both PCC voltage and current are stable before load change, but eventually turn out to be unstable and become oscillating, but M-VSG control strategy can still remain stable during the whole transient process.

HIL experiment results of DFIG rotor speed control and pitch angle regulation are shown from Fig.30 to Fig.32. When DFIG WTG is operating in low wind speed situation, for traditional VSG control strategy, rotor speed is not a direct control subject, so the rotor speed drop is serious, but M-VSG control strategy is able to control rotor speed around the reference value (0.75pu), so that the serious frequency secondary drop can be avoided.

When extra load is cut off from power grid, rotor speed will increase rapidly, which will activate pitch angle regulator, as is shown in Fig.31-32, DFIG pitch angle will increase accordingly, aiming to keep rotor speed constant around 1.2 pu. The above analysis demonstrates that RTDS HIL experiment results can well match the simulation results in the previous section.

VIII. CONCLUSION

In this paper, basic theory of conventional VSG-ISynC control strategy is firstly introduced, then the stability analysis of

VSG-ISynC control strategy is carried out to show that there exists a limited stability boundary for a specific wind speed, active power of DFIG WTG is likely to oscillate and becomes out of control if large load disturbance is added into power system, also the frequency secondary drop is another serious problem, which is harmful to the stable operation of power grid. To solve this problem, a modified VSG-ISynC control strategy is proposed in this paper by dynamically changing the *P-f* droop coefficient of conventional VSG control strategy, aiming to expand the stability boundary of DFIG WTG. Additionally, an extra rotor speed closed loop is added into VSG control strategy, which can significantly reduce serious frequency secondary drop by controlling rotor speed directly. Afterwards, the quantitative analysis and state space equation is built for M-VSG control strategy, impacts of droop coefficient on system stability is investigated by the eigenvalue loci analysis. Finally, a co-simulation and RTDS hardware-in-loop verification are carried out to verify the effectiveness and feasibility of proposed M-VSG control strategy, detailed conclusions are listed as followed:

1) Compared with traditional vector control strategy, VSG-ISynC control strategy is able to provide extra power support to grid, preventing grid frequency from deep drop or increase. This frequency damping ability is similar to that of traditional synchronous generator.
2) For a given wind speed, there exists a minimum rotor speed and a stability boundary, once rotor speed has decreased lower than this value, DFIG WTG will enter the unstable region and become out of control.
3) The proposed M-VSG control strategy is effective in preventing DFIG WTG from entering the unstable region by dynamically changing *P-f* droop coefficient according to the fluctuation of dc link voltage.
4) M-VSG control strategy is also effective in avoiding frequency secondary drop by directly controlling rotor speed. In low wind speed situation, rotor speed control will be activated once it has decreased below the permitted minimum speed. In medium and high wind speed situation, pitch angle regulator will work together with M-VSG control strategy to keep rotor speed operating within a reasonable speed range.

REFERENCES

[1] Q.-C. Zhong, "Power-electronics-enabled autonomous power systems: Architecture and technical routes," *IEEE Trans. Ind. Electron.*, vol. 64, no. 7, pp. 5907–5918, Jul. 2017.
[2] Y. Wu, W. Yang, Y. Hu, and P. Q. Dzung, "Frequency regulation at a wind farm using time-varying inertia and droop controls," *IEEE Trans. Ind. Appl.*, vol. 55, no. 1, pp. 213–224, Feb. 2019.
[3] Z. Wang and W. Wu, "Coordinated control method for DFIG-based wind farm to provide primary frequency regulation service," *IEEE Trans. Power Syst.*, vol. 33, no. 3, pp. 2644–2659, May 2018.
[4] Y. Zhang, A. M. Melin, S. M. Djouadi, M. M. Olama, and K. Tomsovic, "Provision for guaranteed inertial response in diesel-wind systems via model reference control," *IEEE Trans. Power Syst.*, vol. 33, no. 6, pp. 6557–6568, Nov. 2018.
[5] X. Xi, H. Geng, G. Yang, S. Li, and F. Gao, "Torsional oscillation damping control for DFIG-based wind farm participating in power system frequency regulation," *IEEE Trans. Ind. Appl.*, vol. 54, no. 4, pp. 3687–3701, Aug. 2018.
[6] X. Xi, H. Geng, G. Yang, S. Li, and F. Gao, "Two-level damping control for DFIG-based wind farm providing synthetic inertial service," *IEEE Trans. Ind. Appl.*, vol. 54, no. 2, pp. 1712–1723, Apr. 2018.
[7] M. Kayikçi and J. V. Milanovic, "Dynamic contribution of DFIG-based wind plants to system frequency disturbances," *IEEE Trans. Power Syst.*, vol. 24, no. 2, pp. 859–867, May 2009.
[8] O. Anaya-Lara, F. M. Hughes, N. Jenkins, and G. Strbac, "Provision of a synchronising power characteristic on DFIG-based wind farms," *IET Gener., Transmiss. Distrib.*, vol. 1, no. 1, pp. 162–169, Jan. 2007.
[9] Y. Fu, Y. Wang, and X. Zhang, "Integrated wind turbine controller with virtual inertia and primary frequency responses for grid dynamic frequency support," *IET Renew. Power Gener.*, vol. 11, no. 8, pp. 1129–1137, Jun. 2017.
[10] J. A. Suul, S. D'Arco, P. Rodriguez, and M. Molinas, "Extended stability range of weak grids with voltage source converters through impedance-conditioned grid synchronization," in *Proc. 11th IET Int. Conf. AC DC Power Transmiss.*, Birmingham, U.K., Feb. 2015, pp. 1–10.
[11] L.-J. Cai and I. Erlich, "Doubly fed induction generator controller design for the stable operation in weak grids," *IEEE Trans. Sustain. Energy*, vol. 6, no. 3, pp. 1078–1084, Jul. 2015.
[12] Y. Ma, W. Cao, L. F. Yang, F. Wang, and L. M. Tolbert, "Virtual synchronous generator control of full converter wind turbines with short-term energy storage," *IEEE Trans. Ind. Electron.*, vol. 64, no. 11, pp. 8821–8831, Nov. 2017.
[13] J. Liu, Y. Miura, and T. Ise, "Comparison of dynamic characteristics between virtual synchronous generator and droop control in inverter-based distributed generators," *IEEE Trans. Power Electron.*, vol. 31, no. 5, pp. 3600–3611, May 2016.
[14] S. Wang, J. Hu, X. Yuan, and L. Sun, "On inertial dynamics of virtual-synchronous-controlled DFIG-based wind turbines," *IEEE Trans. Energy Convers.*, vol. 30, no. 4, pp. 1691–1702, Dec. 2015.
[15] J. Driesen and K. Visscher, "Virtual synchronous generators," in *Proc. IEEE Power Energy Soc. Gen. Meeting-Convers. Del. Elect. Energy 21st Century*, Feb. 2008, pp. 1–3.
[16] S. Sang, C. Zhang, X. Cai, M. Molinas, J. Zhang, and F. Rao, "Control of a type-IV wind turbine with the capability of robust grid-synchronization and inertial response for weak grid stable operation," *IEEE Access*, vol. 7, pp. 58553–58569, 2019.
[17] H. Shao, X. Cai, D. Zhou, Z. Li, D. Zheng, Y. Cao, Y. Wang, and F. Rao, "Equivalent modeling and comprehensive evaluation of inertia emulation control strategy for DFIG wind turbine generator," *IEEE Access*, vol. 7, pp. 64798–64811, 2019.
[18] W. Wu, L. Zhou, Y. Chen, A. Luo, Y. Dong, X. Zhou, Q. Xu, L. Yang, and J. M. Guerrero, "Sequence-impedance-based stability comparison between VSGs and traditional grid-connected inverters," *IEEE Trans. Power Electron.*, vol. 34, no. 1, pp. 46–52, Jan. 2019.
[19] X. Meng, J. Liu, and Z. Liu, "A generalized droop control for grid-supporting inverter based on comparison between traditional droop control and virtual synchronous generator control," *IEEE Trans. Power Electron.*, vol. 34, no. 6, pp. 5416–5438, Jun. 2019.
[20] L. Huang, H. Xin, L. Zhang, Z. Wang, K. Wu, and H. Wang, "Synchronization and frequency regulation of DFIG-based wind turbine generators with synchronized control," *IEEE Trans. Energy Convers.*, vol. 32, no. 3, pp. 1251–1262, Sep. 2017.
[21] K. Liu, Y. Qu, H.-M. Kim, and H. Song, "Avoiding frequency second dip in power unreserved control during wind power rotational speed recovery," *IEEE Trans. Power Syst.*, vol. 33, no. 3, pp. 3097–3106, May 2018.
[22] L. Xiong, P. Li, F. Wu, and J. Wang, "Stability enhancement of power systems with high DFIG-wind turbine penetration via virtual inertia planning," *IEEE Trans. Power Syst.*, vol. 34, no. 2, pp. 1352–1361, Mar. 2019.

HAOSHU SHAO received the B.Eng. degree in electrical engineering from the China University of Mining and Technology, Xuzhou, China, in 2016. He is currently pursuing the Ph.D. degree in electrical engineering with Shanghai Jiao Tong University, Shanghai, China. His current research interests include modeling and stability analysis of grid-friendly wind turbine integration technology, where the aim is to improve the grid frequency and power stability with the increasing penetration of renewable energies.

XU CAI received the B.Eng. degree in electrical engineering from Southeast University, Nanjing, China, in 1983, and the M.Sc. and Ph.D. degrees from the China University of Mining and Technology, in 1988 and 2000, respectively, where he was an Associate Professor with the Department of Electrical Engineering, from 1989 to 2001.

He joined Shanghai Jiao Tong University, as a Professor, in 2002, where he has been the Director of the Wind Power Research Center, since 2008. His research interests include power electronics and renewable energy exploitation and utilization.

ZHENG LI received the B.Eng. and M.S. degrees in electrical engineering from Southeast University, Nanjing, China, in 1983 and 1986, respectively, and the Ph.D. degree from Donghua University, China, in 2000, where she is currently a Professor of electrical engineering with the School of Information Science and Technology.

She was involved in the areas of power systems, intelligent control, system modeling, wind energy, and battery energy storage systems. Her current research interests include wind energy and micro grid.

DANGSHENG ZHOU received the B.Eng. and M.Sc. degrees in electrical engineering from the Huazhong University of Science and Technology, Wuhan, China, in 1986 and 1999, respectively.

He joined Shenzhen Hopewind Electric Co., Ltd., in 2010. Since 2012, he has been the Director of Research and Development Center. His research interests include renewable energy generation, power electronics equipment development, and control technology research.

SUJUAN SUN received the B.Eng. degree from North China Electric Power University, Baoding, China, in 2005, and the M.Sc. degree from HoHai University, Nanjing, China, in 2017. Since 2005, she has been with the State Grid Electric Power Research Institute (NARI Group Corporation), Nanjing. Her main research interests include wind power generation (such as wide band oscillation, FRT, network adaptability, virtual synchronous generator, electric drive, and energy storage converter control), and generator excitation systems (such as power system stabilizer, and excitation control strategy).

LIANG GUO received the B.Eng. and M.Sc. degrees from the Nanjing University of Aeronautics and Astronautics, Nanjing, China, in 2005 and 2008, respectively. Since 2008, he has been with the State Grid Electric Power Research Institute (NARI Group Corporation), Nanjing. He is currently the Manager of the Wind Power Technology Department, Electric Control Branch. His main research interests include wind power generation (such as FRT, network adaptability, virtual synchronous generator, electric drive, and energy storage converter control) and wind converter hardware and integration technology.

YUNFENG CAO received the M.Sc. and Ph.D. degrees in electrical engineering from the China University of Mining and Technology, Xuzhou, in 2003 and 2006, respectively.

He was a Postdoctoral Research Fellow with the Department of Electrical Engineering, Shanghai Jiao Tong University, Shanghai, China, from 2006 to 2008, where he is currently an Assistant Research Fellow with the Wind Power Research Center. His current research interests include the integration control technology of large scale wind turbine generator.

FANGQUAN RAO received the degree in electrical engineering from the Harbin Institute of Technology, Harbin, China, in 1958. From 1958 to 1966, he was an Electrical Engineer with Harbin Electrical Machinery Works. From 1966 to 1999, he was with Dongfang Electrical Machinery Company Ltd., Deyang, China, where he was the Chief Engineer and a Deputy Director, from 1983 to 1999, and he took part in a number of significant hydro-power projects of China, such as designing generators for power station Longyangxia (320 MW) and organized research on the 300-MW turbo generator and the hydro-generator with evaporation cooling system, which both received the Second Prize of the Chinese National Science and Technology Promotion. In 1999, he joined Shanghai Jiao Tong University, Shanghai, China, where he is currently a Professor with the Electrical Engineering Department. His research interests include the control of large electrical generators and special electrical machines.

Prof. Rao became a member of the Chinese Academy of Engineering, in 1995. He received the First Prize of the Chinese National Science and Technology Promotion from the Chinese Government and the Outstanding Prize of the Science and Technology Promotion of Sichuan Province.